

# Cranked Skyrme–Hartree–Fock–Bogoliubov for a mean-field description of nuclear rotations near the drip line

Kenichi Yoshida<sup>1, \*</sup>

<sup>1</sup>*Department of Physics, Kyoto University, Kyoto, 606-8502, Japan*

(Dated: September 20, 2021)

To describe the yrast states in weakly-bound nuclei, I directly solve the coordinate-space cranked Skyrme–Hartree–Fock–Bogoliubov equation in the quasiparticle basis with the continuum states discretized in a box. After the numerical demonstration for the ground-state band in a medium-mass nucleus, I apply the newly-developed method to neutron-rich even- $N$  Mg isotopes. I find that the appearance of the significantly low-energy  $I^\pi = 2^+$  state in  $^{40}\text{Mg}$  is mainly due to the suppression of pairing. The calculation predicts that the  $2^+$  state in  $^{42}\text{Mg}$  appears as high in energy as in  $^{34-38}\text{Mg}$  whereas the triaxial deformation is enhanced. The present numerical framework offers a practical approach for investigating the near yrast states and revealing structures unique in drip-line nuclei.

A diverse variety of modes of motion show up in nuclei. To explore unique structures in exotic nuclei, various spectroscopic studies have been carried out via decays and making use of direct reactions. Nuclear deformation is a collective phenomenon that has long attracted interest; a nucleus is deformed as it moves away from the magic number due to the many-body correlation. It has been turned out that the shell structure evolves as the conventional magic numbers disappear and new ones appear instead, depending on the combination of the particle numbers of protons and neutrons [1]. Energies of excited nuclear states are often among the first quantities accessible in experiments and have been used as an indicator of the changing shell structure and the onset of deformation [2].

Rotational motion is a manifestation of the spontaneous breaking of the rotational symmetry [3]. The cranking approximation provides an intuitive picture of the rotation of quantum systems, and the cranked shell model is a standard tool to investigate the microscopic structure of nuclear rotations near the ground state and at high spins [4, 5]. The cranked shell model in the framework of the nuclear energy-density functional (EDF) has provided a systematic and quantitative description of the (near) yrast states from light to heavy nuclei [6]. The accumulation of experimental data for low spins in neutron-rich nuclei has stimulated the application of the EDF-based cranked shell model to the elucidation of the rotational motion unique in weakly bound nuclei. Furthermore, it has been pointed out in Ref. [7] that the moments of inertia are sensitive to the pairing and weak binding.

The island of inversion has been the subject of much experimental and theoretical interest [8]. A systematic calculation for the Mg isotopes in the mean-field approximation produces a spherical configuration in  $^{32}\text{Mg}$ , a soft potential energy surface in  $^{34}\text{Mg}$ , and a prolate configuration in  $^{36,38,40}\text{Mg}$  [9]. It has been clarified that the shape fluctuation and the correlation beyond the mean-field approximation is significant in  $^{32}\text{Mg}$  [10–12]. Exper-

imentally, the measurement of not only the first  $I^\pi = 2^+$  state but the  $4^+$  state and their ratio  $R_{4/2} > 3$  have revealed a well-deformed structure in  $^{34,36,38}\text{Mg}$  [13]. The significantly low energy of the  $2^+$  state in  $^{40}\text{Mg}$  is not reproduced by any theoretical models, and it indicates the emergence of a unique feature associated with weak binding [14]. As a coherent contribution of the pairing in the continuum states induces an enhanced transition strength to the low-lying vibrational mode in the Mg isotopes [15–19], the roles of the weak binding and the continuum coupling in the rotational motions are interesting to study.

I investigate in this article the low-spin states in the neutron-rich Mg isotopes close to the drip line. Then, I try to clarify the role of weak binding in the low-lying excited states. To this end, I develop a new framework of the cranked shell model within the nuclear EDF approach, which is capable of handling nuclides with arbitrary mass numbers [6, 20]. To describe the (near) yrast states with proper account of the pairing in the continuum states, I directly solve the coordinate-space cranked Skyrme–Kohn–Sham–Bogoliubov (KSB) or Hartree–Fock–Bogoliubov equation in the quasiparticle basis:

$$\sum_{\sigma'} \begin{bmatrix} h_{\sigma\sigma'}^{q'}(\mathbf{r}) & \tilde{h}_{\sigma\sigma'}^q(\mathbf{r}) \\ 4\sigma\sigma' \tilde{h}_{-\sigma-\sigma'}^{q*}(\mathbf{r}) & -4\sigma\sigma' h_{-\sigma-\sigma'}^{q*}(\mathbf{r}) \end{bmatrix} \begin{bmatrix} \varphi_{1,\alpha}^q(\mathbf{r}\sigma') \\ \varphi_{2,\alpha}^q(\mathbf{r}\sigma') \end{bmatrix} = E'_\alpha \begin{bmatrix} \varphi_{1,\alpha}^q(\mathbf{r}\sigma) \\ \varphi_{2,\alpha}^q(\mathbf{r}\sigma) \end{bmatrix}, \quad (1)$$

which is obtained by extending the formalism developed for describing the ground-state properties of even-even nuclei near the drip line [21]. Here the single-particle Routhian and the pair Hamiltonian are defined by using the Skyrme and pairing EDF  $E[\rho, \tilde{\rho}, \tilde{\rho}^*]$  as  $h_{\sigma\sigma'}^{q'}(\mathbf{r}) = \frac{\delta E[\rho, \tilde{\rho}, \tilde{\rho}^*]}{\delta \rho_{\sigma'\sigma}^{q'}(\mathbf{r})} - (\lambda^q + \omega_{\text{rot}} j_z) \delta_{\sigma\sigma'}$  and  $\tilde{h}_{\sigma\sigma'}^q(\mathbf{r}) = \frac{\delta E[\rho, \tilde{\rho}, \tilde{\rho}^*]}{\delta \tilde{\rho}_{\sigma'\sigma}^{q*}(\mathbf{r})}$ . I define the  $z$ -axis as a quantization axis of the intrinsic spin and consider the system rotating uniformly about the  $z$ -axis. I take the natural units:  $\hbar = c = 1$ .

The numerical procedure to solve Eq. (1) is basically the same as in solving the cranked KS equation in Refs. [22, 23]. I impose the reflection symmetry about

\* E-mail: [kyoshida@ruby.scphys.kyoto-u.ac.jp](mailto:kyoshida@ruby.scphys.kyoto-u.ac.jp)

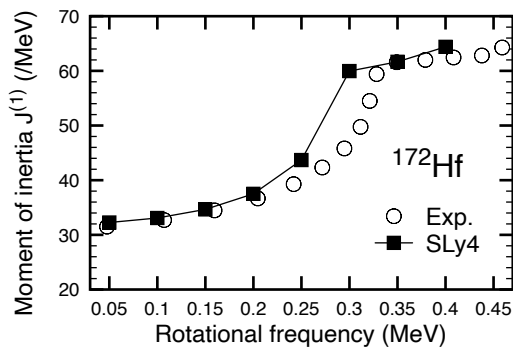


FIG. 1. Kinematic moments of inertia  $\mathcal{J}^{(1)}$  as functions of the rotational frequency. The experimental data [30] are denoted by open symbols.

the  $(x, y)$ -,  $(y, z)$ - and  $(z, x)$ -planes. Thus, the parity  $\mathbf{p}_k$  ( $= \pm 1$ ) and  $z$ -signature  $r_k$  ( $= \pm i$ ) are a good quantum number. I solve Eq. (1) by diagonalizing the KSB Hamiltonian in the three-dimensional (3D) Cartesian-mesh representation with the box boundary condition. Thanks to the reflection symmetries, I have only to consider explicitly the octant region in space with  $x \geq 0$ ,  $y \geq 0$ , and  $z \geq 0$ ; see Refs. [24, 25] for details. I use a 3D lattice mesh  $x_i = ih - h/2$ ,  $y_j = jh - h/2$ ,  $z_k = kh - h/2$  ( $i, j, k = 1, 2, \dots, M$ ) with a mesh size  $h = 1.0$  fm and  $M = 10$  for each direction. To check the convergence of the results with respect to the box size and to investigate the effect of the weak binding, I change  $M$  in the discussion below. The differential operators are represented by the use of the 9-point formula of the finite difference method. For diagonalization of the matrix of Eq. (1), I use the LAPACK DSYEVX subroutine [26]. A modified Broyden's method [27] is utilized to calculate new densities during the selfconsistent iteration. The quasiparticle Routhians are cut off at 60 MeV.

To see the validity of the present framework, I perform the calculation for the ground-state rotational band in  $^{172}\text{Hf}$  as a typical example of the collective rotation. Figure 1 shows the calculated kinematic moments of inertia  $\mathcal{J}^{(1)}$  as functions of the rotational frequency. I employed the SLy4 [28] and the Yamagami-Shimizu-Nakatsukasa (YSN) pairing EDF in Ref. [29]. The present model describes well the low spin states and the band crossing. Around  $\omega_{\text{rot}} = 0.25$  MeV, the alignment of neutrons in the  $i_{13/2}$  orbital occurs, whereas this is lower than the measurement  $\sim 0.3$  MeV. One sees that the rotational property beyond the band crossing is also reasonably described.

Then, I investigate the low-spin yrast states in the neutron-rich Mg isotopes. I use the SkM\* functional [32] and the so-called mixed-type pairing interaction with the strength  $V_0 = -295$  MeV fm<sup>3</sup> as in Ref. [18]. The ground-state properties thus obtained are summarized in Table 1 of Ref. [18]. I found that the triaxiality is negligibly small:  $\gamma < 1^\circ$  in low spins. Be-

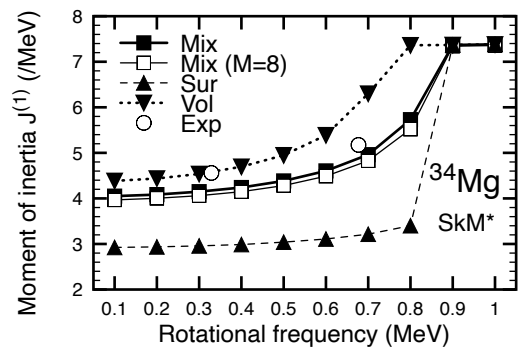


FIG. 2. Similar to Fig. 1 but for  $^{34}\text{Mg}$ . The results obtained by using several pairing interactions are displayed. The experimental data are obtained from Ref. [31].

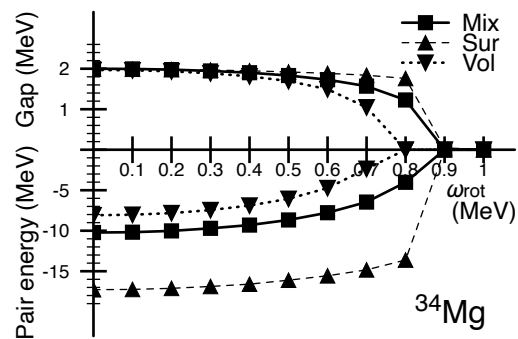


FIG. 3. Absolute value of the pairing gaps  $|\Delta|$  and pairing energies  $E_{\text{pair}}$  of neutrons in  $^{34}\text{Mg}$ .

cause the chemical potential is a key quantity governing the spatial structure of quasiparticle wave functions, I put it down:  $-4.17, -3.25, -2.41, -1.60$  MeV for neutrons in  $^{34,36,38,40}\text{Mg}$ , respectively. When the two-basis method, in which the KSB Hamiltonian is diagonalized in a truncated single-particle basis [6], is employed for such weakly-bound nuclei, the single-particle continuum states enter the pairing window. Therefore, the convergence with respect to the number of basis states has to be carefully examined because the densities should be spatially localized as far as  $\lambda < 0$ . In the present case, however, the densities are always calculated to be localized because the full KSB Hamiltonian is directly diagonalized [21].

Figure 2 shows the calculated  $\mathcal{J}^{(1)}$  of  $^{34}\text{Mg}$ , and compares with the experimental data [31]. The measured  $R_{4/2}$  value is 3.06, which is marginally lower than that of the rigid rotor. The calculation reproduces well the slight increase in  $\mathcal{J}^{(1)}$  due to the weakening of pairing. The role of the density dependence of the pairing interaction has been discussed in the study of the superdeformed states [33]: the density dependence results in a retarded alignment. I investigate here the density dependence of the pairing interaction in the light nuclei.

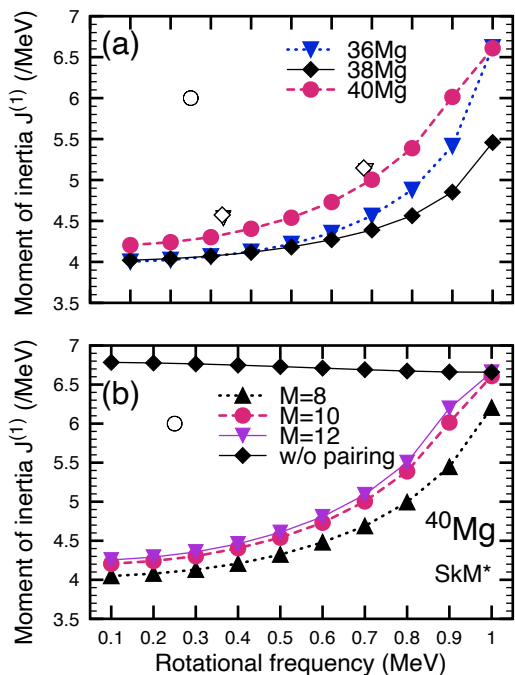


FIG. 4. (a) Similar to Fig. 1 but for  $^{36,38,40}\text{Mg}$ . The experimental data, open symbols, are taken from Refs. [13, 14]. (b) Calculated  $\mathcal{J}^{(1)}$  for  $^{40}\text{Mg}$  obtained with the box size of  $M = 8, 10$ , and  $12$ . Results without the pairing are also depicted.

To this end, I use the volume- and surface-type pairing interactions. I determined the strength to keep the calculated pairing gap as obtained with the mixed pairing:  $V_0 = -207$  and  $-451$  MeV fm $^3$  for the volume and surface pairing, respectively. The pairing gap is defined as  $\Delta^q = \int dr \tilde{h}^q(\mathbf{r}) \rho^q(\mathbf{r}) / \int dr \rho^q(\mathbf{r})$  and the resultant gap is shown in Fig. 3. Notice that the protons are unpaired at  $\omega_{\text{rot}} = 0$ . In low  $\omega_{\text{rot}}$ , the volume pairing also reproduces the experimental value. However, it gives a faster increase in  $\mathcal{J}^{(1)}$  similarly to the finding in Ref. [33]. The surface pairing shows a slow increase in  $\mathcal{J}^{(1)}$ . An interesting feature is that the magnitude of  $\mathcal{J}^{(1)}$  is inversely proportional to the magnitude of the pairing energy  $E_{\text{pair}}^q = 1/2 \int dr \tilde{h}^q(\mathbf{r}) \tilde{\rho}^{q*}(\mathbf{r})$ , as shown in Fig. 3.

Next, I investigate the rotational property of  $^{36,38,40}\text{Mg}$  located close to the drip line. Figure 4(a) displays the calculated  $\mathcal{J}^{(1)}$  together with the experimental data [13, 14]. The calculated  $\mathcal{J}^{(1)}$  for  $^{36,38}\text{Mg}$  in low  $\omega_{\text{rot}}$  is similar to the one for  $^{34}\text{Mg}$ , and smaller than that for  $^{40}\text{Mg}$ . This is consistent with the calculation in Ref. [18], where the moments of inertia were evaluated using the Thouless-Valatin procedure in the framework of the Skyrme EDF-based QRPA [34]. A higher value for  $\mathcal{J}^{(1)}$  of  $^{40}\text{Mg}$  is partly because of smaller deformation than others. Another reason is the weak-binding effect, as discussed below. The experimental data indicate that the pairing in  $^{36,38}\text{Mg}$  would be weaker than the calculation because the

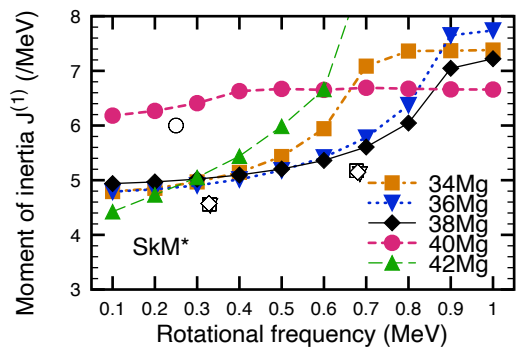


FIG. 5. Similar to Fig. 1 but for  $^{34,36,38,40}\text{Mg}$  obtained using the YSN pairing functional of Ref. [29].

measured  $\mathcal{J}^{(1)}$  is slightly larger than the calculated one. Furthermore, the measurement shows a faster increase in  $\mathcal{J}^{(1)}$  than the calculation for  $^{38}\text{Mg}$ ; the calculation produces a stronger pairing correlation. As in the case of  $^{34}\text{Mg}$ , I found a good correspondence between  $\mathcal{J}^{(1)}$  and  $E_{\text{pair}}$ .

The present calculation fails to describe the rotational motion in  $^{40}\text{Mg}$ : the calculated  $\mathcal{J}^{(1)}$  is far below the measured value. One is then tempted to expect that the weak-binding effect shows up. In Fig. 4(b), I show the results obtained by varying the box size. With the increase in the box size, the calculated  $\mathcal{J}^{(1)}$  increases. The calculation with  $M = 8$  does not show the convergence, while the difference between the results with  $M = 10$  and  $12$  becomes small. One cannot expect a further increase in  $\mathcal{J}^{(1)}$  even enlarging the box size. Notice that for the case of  $^{34}\text{Mg}$ , the results obtained with  $M = 8$  and  $10$  are not very different, as shown in Fig. 2. In this sense, the weak-binding effect appears in  $^{40}\text{Mg}$ ; the weak binding of neutrons reduces the pairing correlation and enhances the moment of inertia. As an extreme case of weak pairing, I performed the calculation without the pairing, as displayed in Fig. 4(b). The resultant  $\mathcal{J}^{(1)}$  is much larger than that obtained with pairing. As increasing the rotational frequency, the results with and without pairing become closer to each other. The observed  $\mathcal{J}^{(1)}$  of  $6.0$  MeV $^{-1}$  is between these results and is relatively closer to the one obtained without pairing  $\mathcal{J}^{(1)} = 6.8$  MeV $^{-1}$ . As pointed out in Ref. [9], one has an oblate minimum in  $^{40}\text{Mg}$ . Indeed, I found the oblate solution with  $\beta = 0.16, \gamma = 60^\circ$ . With this configuration, the resultant  $\mathcal{J}^{(1)}$  is much lower:  $1.6$  MeV $^{-1}$ .

To describe the isotopic dependence of low-spin states in the Mg isotopes, a key is the isospin dependence of the pairing correlation. Thus, I employ the optimal pairing EDF, the YSN functional [29], in which the isovector-density dependence is introduced to describe pairing in neutron-rich nuclei. Figure 5 shows the calculated  $\mathcal{J}^{(1)}$  in  $^{34-42}\text{Mg}$ . Since the coupling constant of the YSN pairing functional was fixed for the rare-earth nuclei, it gives a weak pairing in light nuclei: the density of single-particle

states near the Fermi energy is low. The calculated  $\mathcal{J}^{(1)}$  are thus all larger than those obtained with the mixed pairing. The pairing vanishes at as low as  $\omega_{\text{rot}} = 0.8$  MeV and 0.5 MeV in  $^{34}\text{Mg}$  and  $^{40}\text{Mg}$ , respectively. However, the enhancement in  $\mathcal{J}^{(1)}$  from  $^{38}\text{Mg}$  to  $^{40}\text{Mg}$  is well described. One sees the enhancement by 28% at  $\omega_{\text{rot}} = 0.3$  MeV, which is comparable to the experimental observation of the lowering in the  $2_1^+$  energy from  $^{38}\text{Mg}$  to  $^{40}\text{Mg}$  by 23% [14]. When the SLy4 functional is employed together with the YSN pairing functional, both neutrons and protons are unpaired in  $^{40}\text{Mg}$ , while neutrons are paired in  $^{38}\text{Mg}$ . Therefore, a significant lowering of the excitation energy of  $2_1^+$  state in  $^{40}\text{Mg}$  is also described.

When two neutrons are added, I find a further structural change. Comparing with  $^{40}\text{Mg}$ , the deformation gets weaker by about 33%, and the triaxiality develops. The pairing for protons shows up, and that for neutrons increases. Accordingly,  $\mathcal{J}^{(1)}$  is reduced as shown in Fig. 5. The yrast band terminates at  $\omega_{\text{rot}} = 0.8$  MeV, reaching  $\mathcal{J}^{(1)} = 11$  MeV $^{-1}$ . Therefore, the present calculation with SkM\*+YSN predicts that the irregularity in the  $2_1^+$  state appears only at  $^{40}\text{Mg}$ . I found that the calculated  $\mathcal{J}^{(1)}$  changes by about 2% when the box size is varied from  $M = 10$  to 12. Investigation of the halo structure in such a triaxially-deformed rotating nucleus is an interesting future work though it needs a larger box [35].

To summarize, I have developed a numerical framework for a mean-field description of near yrast states in

nuclei near the drip line in a nuclear EDF approach. I directly solved the coordinate-space cranked Skyrme-KSB equation in the quasiparticle basis, with the continuum states being discretized in a box. The present framework reproduces the low-spin states and band crossing in a medium-heavy deformed nucleus.

The low-spin states in  $^{34}\text{Mg}$  are well described by using the density-dependent pairing interaction. The calculated moments of inertia show the inverse correlation with the magnitude of the pairing energy; the moments of inertia increase as the magnitude of pairing energy decreases. With the increase in the neutron number, the calculation overestimates the pairing correlation, thus leading to the underestimation of the moments of inertia. Employing the pairing EDF constructed to describe the isospin dependence in neutron-rich nuclei, I have found that the appearance of the significantly low-energy  $I^\pi = 2^+$  state in  $^{40}\text{Mg}$  is mainly due to the suppression of pairing. In  $^{42}\text{Mg}$ , the  $2_1^+$  state appears higher in energy than in  $^{40}\text{Mg}$  due to the structure change.

## ACKNOWLEDGMENTS

This work was supported by the JSPS KAKENHI (Grants No. JP19K03824 and No. JP19K03872). The numerical calculations were performed on the computing facilities at the Yukawa Institute for Theoretical Physics, Kyoto University, and at the Research Center for Nuclear Physics, Osaka University.

- 
- [1] T. Otsuka, A. Gade, O. Sorlin, T. Suzuki, and Y. Utsuno, Evolution of shell structure in exotic nuclei, *Rev. Mod. Phys.* **92**, 015002 (2020).
  - [2] A. Gade, Excitation energies in neutron-rich rare isotopes as indicators of changing shell structure, *Eur. Phys. J. A* **51**, 118 (2015).
  - [3] A. Bohr and B. Mottelson, *Nuclear Structure: Volume II, Nuclear Deformations* (Benjamin, Reading, MA, 1975).
  - [4] P. Ring, R. Beck, and H. J. Mang, On the application of the Hartree-Fock-Bogolyubov-equations to a microscopic theory of nuclear rotations, *Z. Phys. A* **231**, 10 (1970).
  - [5] R. Bengtsson, S. Frauendorf, and F.-R. May, Quasiparticle levels in rotating rare earth nuclei: A cranked shell-model dictionary, *At. Data Nucl. Data Tab.* **35**, 15 (1986).
  - [6] M. Bender, P.-H. Heenen, and P.-G. Reinhard, Self-consistent mean-field models for nuclear structure, *Rev. Mod. Phys.* **75**, 121 (2003).
  - [7] M. Yamagami and Y. R. Shimizu, Pairing effects for rotational excitations unique to neutron-rich nuclei, *Phys. Rev. C* **77**, 064319 (2008).
  - [8] O. Sorlin and M.-G. Porquet, Nuclear magic numbers: New features far from stability, *Prog. Part. Nucl. Phys.* **61**, 602 (2008).
  - [9] J. Terasaki, H. Flocard, P.-H. Heenen, and P. Bonche, Deformation of nuclei close to the two-neutron drip line in the Mg region, *Nucl. Phys. A* **621**, 706 (1997).
  - [10] M. Kimura and H. Horiuchi, Breaking of the Neutron Magic Number  $N = 20$  in  $^{32}\text{Mg}$  and  $^{30}\text{Ne}$  and Its Possible Relation to the Cluster Structure, *Prog. Theor. Phys.* **107**, 33 (2002), <https://academic.oup.com/ptp/article-pdf/107/1/33/5213174/107-1-33.pdf>.
  - [11] R. Rodríguez-Guzmán, J. Egido, and L. Robledo, Correlations beyond the mean field in magnesium isotopes: angular momentum projection and configuration mixing, *Nucl. Phys. A* **709**, 201 (2002).
  - [12] N. Hinohara, K. Sato, K. Yoshida, T. Nakatsukasa, M. Matsuo, and K. Matsuyanagi, Shape fluctuations in the ground and excited  $0^+$  states of  $^{30,32,34}\text{Mg}$ , *Phys. Rev. C* **84**, 061302 (2011).
  - [13] P. Doornenbal, H. Scheit, S. Takeuchi, N. Aoi, K. Li, M. Matsushita, D. Steppenbeck, H. Wang, H. Baba, H. Crawford, C. R. Hoffman, R. Hughes, E. Ideguchi, N. Kobayashi, Y. Kondo, J. Lee, S. Michimasa, T. Motobayashi, H. Sakurai, M. Takechi, Y. Togano, R. Winkler, and K. Yoneda, In-Beam  $\gamma$ -Ray Spectroscopy of  $^{34,36,38}\text{Mg}$ : Merging the  $N=20$  and  $N=28$  Shell Quenching, *Phys. Rev. Lett.* **111**, 212502 (2013).
  - [14] H. L. Crawford, P. Fallon, A. O. Macchiavelli, P. Doornenbal, N. Aoi, F. Browne, C. M. Campbell, S. Chen, R. M. Clark, M. L. Cortés, M. Cromaz, E. Ideguchi, M. D. Jones, R. Kanungo, M. MacCormick, S. Momiyama, I. Murray, M. Niikura, S. Paschalis, M. Petri, H. Sakurai, M. Salathe, P. Schrock, D. Steppen-

- beck, S. Takeuchi, Y. K. Tanaka, R. Taniuchi, H. Wang, and K. Wimmer, First Spectroscopy of the Near Drip-line Nucleus  $^{40}\text{Mg}$ , *Phys. Rev. Lett.* **122**, 052501 (2019).
- [15] K. Yoshida, M. Yamagami, and K. Matsuyanagi, Pairing and continuum effects on low-frequency quadrupole vibrations in deformed Mg isotopes close to the neutron drip line, *Nucl. Phys. A* **779**, 99 (2006), [arXiv:nucl-th/0605073](#).
- [16] K. Yoshida, M. Yamagami, and K. Matsuyanagi, Dynamic pairing effects on low-frequency modes of excitation in deformed Mg isotopes close to the neutron drip line, *Phys. Scr. T* **125**, 45 (2006), [arXiv:nucl-th/0507047](#).
- [17] K. Yoshida and M. Yamagami, Low-frequency  $K^\pi = 0^+$  modes in deformed neutron-rich nuclei: Pairing- and  $\beta$ -vibrational modes of neutron, *Phys. Rev. C* **77**, 044312 (2008), [arXiv:0802.2341 \[nucl-th\]](#).
- [18] K. Yoshida, Skyrme-QRPA calculations for low-lying excitation modes in deformed neutron-rich nuclei, *Eur. Phys. J. A* **42**, 583 (2009), [arXiv:0902.3053 \[nucl-th\]](#).
- [19] M. Yamagami, Pairing effect on  $K^\pi = 0^+$  quadrupole excitations in neutron-rich Mg isotopes studied by Skyrme quasiparticle random-phase approximation calculations in wave-number space, *Phys. Rev. C* **100**, 054302 (2019).
- [20] T. Nakatsukasa, K. Matsuyanagi, M. Matsuo, and K. Yabana, Time-dependent density-functional description of nuclear dynamics, *Rev. Mod. Phys.* **88**, 045004 (2016), [arXiv:1606.04717](#).
- [21] J. Dobaczewski, H. Flocard, and J. Treiner, Hartree-Fock-Bogolyubov description of nuclei near the neutron drip line, *Nucl. Phys. A* **422**, 103 (1984).
- [22] S. Sakai, K. Yoshida, and M. Matsuo, Signature dependent triaxiality for shape evolution from superdeformation in rapidly rotating  $^{40}\text{Ca}$  and  $^{41}\text{Ca}$ , *Prog. Theor. Exp. Phys.* **2020**, 063D02 (2020), [arXiv:2003.06081 \[nucl-th\]](#).
- [23] K. Yoshida, Competing shell effect of protons and neutrons for superdeformation in  $^{60}\text{Zn}$ ,  $^{62}\text{Zn}$ , and  $^{64}\text{Ge}$ , (2021), [arXiv:2108.12130 \[nucl-th\]](#).
- [24] P. Bonche, H. Flocard, and P. Heenen, Self-consistent calculation of nuclear rotations: The complete yrast line of  $^{24}\text{Mg}$ , *Nucl. Phys. A* **467**, 115 (1987).
- [25] H. Ogasawara, K. Yoshida, M. Yamagami, S. Mizutori, and K. Matsuyanagi, Rotational Frequency Dependence of Octupole Vibrations on Superdeformed States in  $^{40}\text{Ca}$ , *Prog. Theor. Phys.* **121**, 357 (2009).
- [26] E. Anderson, Z. Bai, C. Bischof, S. Blackford, J. Demmel, J. Dongarra, J. Du Croz, A. Greenbaum, S. Hammarling, A. McKenney, and D. Sorensen, *LAPACK Users' Guide*, 3rd ed. (Society for Industrial and Applied Mathematics, Philadelphia, PA, 1999).
- [27] A. Baran, A. Bulgac, M. M. Forbes, G. Hagen, W. Nazarewicz, N. Schunck, and M. V. Stoitsov, Broyden's method in nuclear structure calculations, *Phys. Rev. C* **78**, 014318 (2008).
- [28] E. Chabanat, P. Bonche, P. Haensel, J. Meyer, and R. Schaeffer, A Skyrme parametrization from subnuclear to neutron star densities. 2. Nuclei far from stabilities, *Nucl. Phys. A* **635**, 231 (1998), [Erratum: *Nucl. Phys. A* 643, 441–441 (1998)].
- [29] M. Yamagami, Y. R. Shimizu, and T. Nakatsukasa, Optimal pair density functional for description of nuclei with large neutron excess, *Phys. Rev. C* **80**, 064301 (2009), [arXiv:0812.3197 \[nucl-th\]](#).
- [30] National Nuclear Data Center, "Evaluated Nuclear Structure Data File", <https://www.nndc.bnl.gov/ensdf/>.
- [31] S. Michimasa, Y. Yanagisawa, K. Inafuku, N. Aoi, Z. Elekes, Z. Fülöp, Y. Ichikawa, N. Iwasa, K. Kurita, M. Kurokawa, T. Machida, T. Motobayashi, T. Nakamura, T. Nakabayashi, M. Notani, H. J. Ong, T. K. Onishi, H. Otsu, H. Sakurai, M. Shinohara, T. Sumikama, S. Takeuchi, K. Tanaka, Y. Togano, K. Yamada, M. Yamaguchi, and K. Yoneda, Quadrupole collectivity in island-of-inversion nuclei  $^{28,30}\text{Ne}$  and  $^{34,36}\text{Mg}$ , *Phys. Rev. C* **89**, 054307 (2014).
- [32] J. Bartel, P. Quentin, M. Brack, C. Guet, and H.-B. Håkansson, Towards a better parametrisation of Skyrme-like effective forces: A critical study of the SkM force, *Nucl. Phys. A* **386**, 79 (1982).
- [33] J. Terasaki, P.-H. Heenen, P. Bonche, J. Dobaczewski, and H. Flocard, Superdeformed rotational bands with density dependent pairing interactions, *Nucl. Phys. A* **593**, 1 (1995).
- [34] K. Yoshida and N. Van Giai, Deformed quasiparticle-random-phase approximation for neutron-rich nuclei using the Skyrme energy density functional, *Phys. Rev. C* **78**, 064316 (2008), [arXiv:0809.0169 \[nucl-th\]](#).
- [35] K. Uzawa, K. Hagino, and K. Yoshida, Role of triaxiality in deformed halo nuclei, *Phys. Rev. C* **104**, L011303 (2021), [arXiv:2104.02946 \[nucl-th\]](#).